# Experimental constraints on the differentiation of low-alkali magmas beneath the Tonga arc: Implications for the origin of arc tholeiites

C. Firth, J. Adam, S. Turner, T. Rushmer, R. Brens, T. G. Green, Saskia Erdmann, H. O'Neill

# Experimental constraints on the differentiation of low-alkali magmas beneath the Tonga arc: Implications for the origin of arc tholeiites

C. Firth [a,] , J. Adam [a], S. Turner [a], T. Rushmer [a], R. Brens [a], T.H. Green [a], S. Erdmann [b], H. O'Neill [c]

[a] Department of Earth and Planetary Science, Macquarie University, North Ryde, NSW, Australia
[b] Institut des Sciences de la Terre d'Orléans (ISTO), Université d'Orléans, CNRS, BRGM, UMR 7327 1a Rue de la Férollerie, 45071 Orléans, France
[c] Research School of Earth Science, Australian National University, Canberra, ACT, Australia

Keywords:
Tonga-Kermadec
Tholeiite
Crystal fractionation
Experimental petrology

## abstract

Hydrous melting experiments on a basaltic andesite from Late Volcano in the Tonga Arc were conducted at 900– 1250 °C and 1 atm to 2.5 GPa, with a range of added $H_2O$ concentrations (0–9 wt%). These were used to constrain conditions of phenocryst precipitation in the basaltic andesite and to better understand the processes of mag-matic differentiation beneath Tongan volcanoes. Comparison between the products of experiments and Tongan lavas indicates that basaltic andesites from Late crystallised plagioclase + augite + pigeonite ± orthopyroxene while water-saturated at comparatively low pressures (≤0.2 GPa) but high temperatures (≥1000 °C). Glasses produced at 950 °C and 0.2 GPa are similar in composition to dacites from neighbouring vol-canoes, including Fonualei. This confirms previous interpretations of dacite magma genesis by crystal fraction-ation of plagioclase and clinopyroxene from basaltic andesite parent magmas, rather than by partial melting of lower crust. This produces decreases in Dy/Yb with increasing $SiO_2$ without a role for amphibole, probably due to the high temperatures and low alkali concentrations involved. Tongan magmas are primarily tholeiitic, and their high water contents bring into question previous hypotheses that attribute the tholeiitic trend to low con-centrations of magmatic $H_2O$. Attributes inherited from the Tongan parent magmas, including low alkali concen-trations, appear to drive tholeiitic differentiation, regardless of water content.

## 1. Introduction

Magmas erupted in subduction settings are rarely primary melts, having been influenced by a range of processes that include crystal frac-tionation, mixing of magmatic materials (liquids, crystals, xenoliths and enclaves), degassing, and reaction between magmas and wall rocks. These processes influence the compositions of derivative magmas, which in-turn affect eruption style. A point of debate centres on the depths at which magmas stall and differentiate. Proposed depths of dif-ferentiation have ranged from the crust-mantle boundary (e.g. Annen et al., 2006) to the shallow upper crust (e.g. Adam et al., 2016). The depth of magma storage has significant implications for the processes that control magmatic differentiation and contribute to the formation of continental crust. For example, partial melting and assimilation of the crust is invoked to a much greater degree in the deep crustal storage hypothesis. Intra-oceanic, island arc systems provide a natural labora-tory to study these processes due to the absence of significantly older and previously differentiated crust.

The Tonga-Kermadec system has long been recognised as an ideal location for the study of intra-oceanic arcs (e.g. Smith and Price, 2006 and references therein). It is for this reason that we conducted hydrous melting experiments on a natural basaltic andesite from Late Volcano in the Tonga Arc. These experiments have been used to examine the con-ditions and processes of magma evolution from basaltic andesite through to dacite in the Tonga Arc, which is the focus of this study. Pioneering studies by Ewart and colleagues have already documented the volcanology, petrography and to a lesser extent the geochemistry of emergent volcanic islands in the Tonga Arc (e.g. Bryan et al., 1972; Ewart et al., 1973). More recent studies have provided comprehensive geochemical datasets for volcanic rocks from Tofua, Fonualei, Kao, Late, Niuatoputapu and Tafahi (Beier et al., 2017; Caulfield et al., 2012; Turner et al., 2012). These allow direct comparison between a selection of Tongan volcanic samples and the experiments presented here.

The Tonga Arc is of additional interest to experimental petrologists because it erupts magmas that are of tholeiitic composition (e.g. Ewart et al., 1973). To date, the majority of experimental studies of arc rocks have focused on calc-alkaline suites from continental arcs (e.g. Blatter et al., 2013; Grove et al., 2003; Nandedkar et al., 2014) whereas recent experimental studies of tholeiitic volcanics from intra-oceanic arcs are far less common (although see Nicholls and Ringwood, 1973; Hamada et al., 2014). Consequently, we use the results from our study to exam-ine not only conditions of magma differentiation, but also the influence of these conditions on the evolution of the tholeiitic trend in arc

Corresponding author.
E-mail address: christopher.firth@mq.edu.au (C. Firth).

magmas. The latter has been ascribed to a range of factors, including crustal thickness (Farner and Lee, 2017; Green, 1980), concentrations of magmatic water (Hamada and Fujii, 2008; Nicholls and Ringwood, 1973; Parman et al., 2011; Tatsumi and Suzuki, 2009; Zimmer et al., 2010) and oxygen fugacity (e.g. Brounce et al., 2014). Here, it will be ar-gued that the tholeiitic trend of the Tongan magmas is not related to water concentrations, but is instead primarily the result of parent magmas that were depleted in alkalis, but enriched in Si and Fe. We sug-gest that these parent melts fractionated to produce basaltic andesites and eventually dacites under shallow (≤ 0.2 GPa) $H_2O$-saturated conditions.

### 1.1. Tectonic and geological setting

The 2500 km-long, intra-oceanic Tonga-Kermadec Arc is located in the south-west Pacific Ocean and marks the westward subduction of the Pacific Plate beneath the Australian Plate (Fig. 1). The active arc is bound to the east by the Tonga-Kermadec Trench and to the west by ex-tensional back-arc rifts of the Havre Trough and Lau Basin. The Louisville Seamount Chain intersects the trench at ~26.5°S, delineating the Tonga and Kermadec portions of the arc (Smith and Price, 2006). Convergence rates reach a global maximum at the northern end of the arc (~240 mm/yr) and decrease southwards. Adjacent to Late, convergence rates are ~200 mm/yr (Bevis et al., 1995). The crustal thickness of the Tongan Arc is ~16 km (Contreras-Reyes et al., 2011).

Late is a currently active island volcano located at 18.8°S within the central Tongan Arc (Fig. 1). It is constructed from inter-bedded basaltic andesite and andesite lava flows and scoria deposits (Bryan et al., 1972; Ewart et al., 1973; Turner et al., 2012) indicating both effusive and ex-plosive phases of eruption (Bryan et al., 1972). The most recent erup-tions occurred in 1790 and 1854 CE Bryan et al. (1972) observed weak solfataric activity during their visit in 1968. Although dacites have not

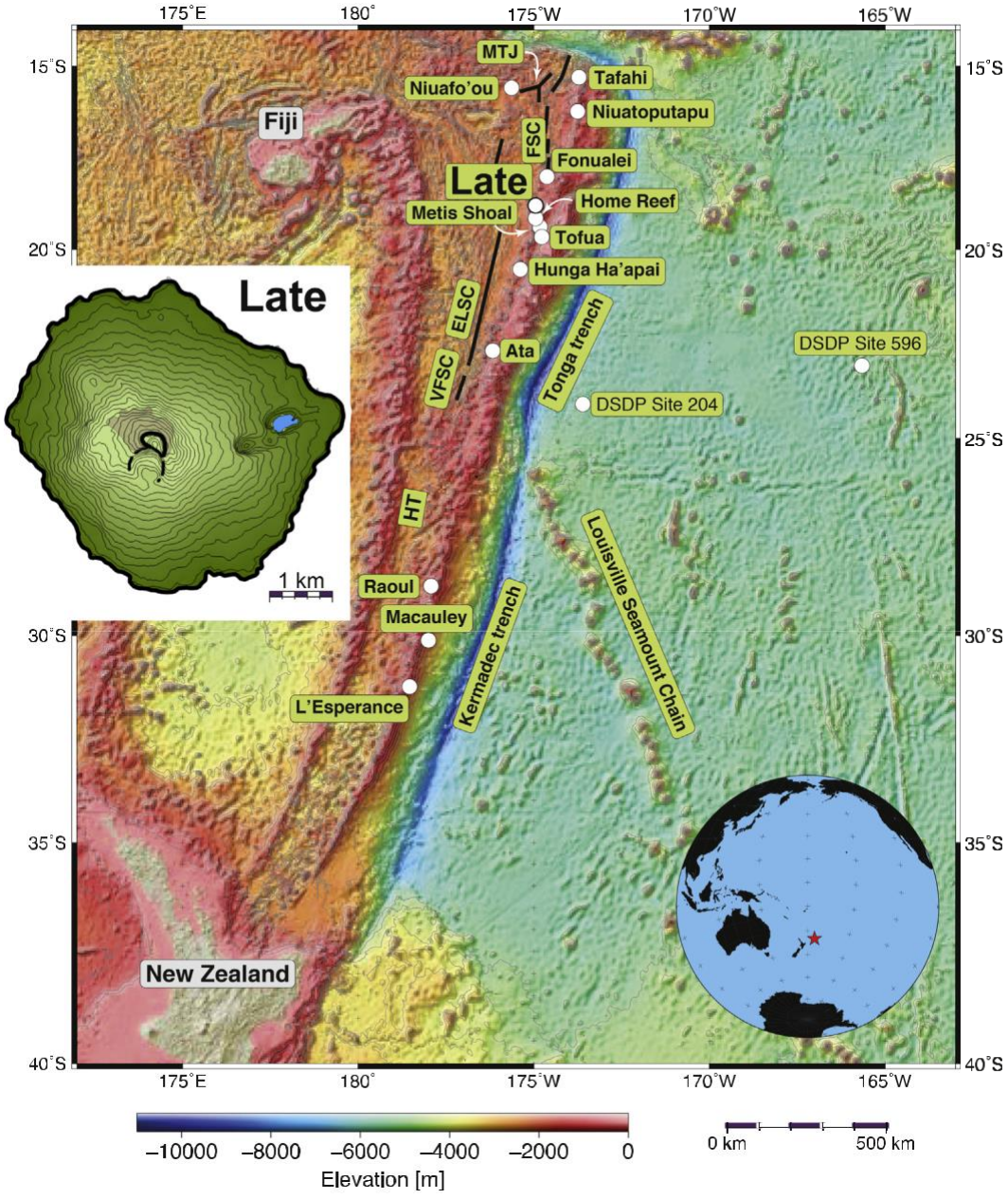


Fig. 1. Map of the Tonga-Kermadec Arc system, showing the location of Late Volcano, which is magnified on the left. HT – Havre Trough; MTJ – Mangatolo Triple Junction; FSC – Fonualei Spreading Centre; The Lau Basin (not marked) consists of the Eastern Lau (ELSC) and Valu Fa (VFSC) spreading centres. Bathymetric map produced using Generic Mapping Tools (GMT) software.

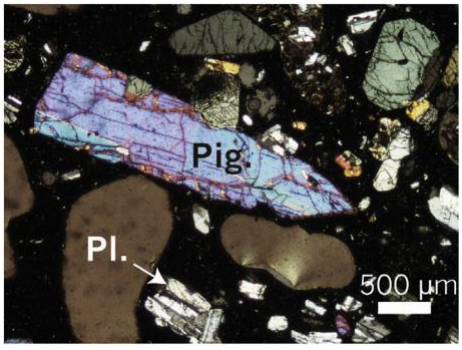


Fig. 2. A photomicrograph showing a typical lava from Late (sample L2).

been found on Late they are recorded at other Tongan volcanoes, most notably adjacent Fonualei where they overlie basaltic andesites similar to those found on Late and Tofua (Caulfield et al., 2012; Turner et al., 2012).

The Late lavas follow a low-K tholeiitic evolutionary trend. They typ-ically contain between 2.5 and 30% of phenocrysts (Fig. 2) that include plagioclase (~2–25%), clinopyroxene (including both augite and pigeon-ite - ~0.5–15%) and orthopyroxene (~0.3–0.5%) (Ewart et al., 1973). Similar phenocryst assemblages are observed in volcanic rocks from neighbouring islands (Caulfield et al., 2012; Ewart et al., 1973; Turner et al., 2012). Plagioclase phenocrysts in the Late samples are highly cal-cic ($An_{N85}$) (Ewart et al., 1973) consistent with values typical of island arc tholeiites (e.g. Hamada et al., 2014; Kuno, 1968). Titanomagnetite is largely absent from the Late samples, but is observed in the more si-licic andesites and dacites from neighbouring islands, including Fonualei (Ewart et al., 1973). Pre-eruptive $H_2O$ concentrations have not been determined for the Late samples, however Caulfield et al. (2012) report $H_2O$ concentrations of 4.16 wt% in melt inclusions hosted by clinopyroxene phenocrysts in basaltic andesites from Tofua. These measurements provide the best estimate for water contents in Late magmas, given the similarity in geochemistry and petrology of lavas erupted from Tofua and Late (Caulfield et al., 2012; Ewart et al., 1973). Furthermore, similar $H_2O$ concentrations (2.34–4.66 wt%) have been re-ported from a range of submarine volcanoes in the Tonga arc (Cooper et al., 2012).

With regard to the time scales of magmatic processes, lavas from Late Volcano have large U- and Ra-excesses (Turner et al., 2003, 2012), which imply magma transit times from slab to surface of b1 kyr (Caulfield et al., 2012). A combined U-series and crystal size distri-bution analysis of sample Late 2 suggests that ~4% of the plagioclase crystal population was inherited from pre-existing cumulates (Turner et al., 2003). These crystals likely took ~400 years to grow but may have been stored in a cumulate pile for up to 50,000 years prior to remobilisation in a subsequent magma batch. Smaller phenocrysts took ~140 years to grow and had a magma residence time of ~1700 years (Turner et al., 2003).

## 2. Experimental and analytical methods

Hydrous melting experiments were conducted at 900–1242 °C and 1 atm to 2.5 GPa, with a range of $H_2O$ concentrations (0–9 wt %) added to the starting material. The latter was a powdered glass prepared from a natural basaltic andesite (L1) from Late (Table 1). This starting material was the subject of an older (unpublished) ex-perimental study by TH Green that involved a systematic investiga-tion of the liquidus and sub-liquidus equilibria of L1 under hydrous conditions (with 5 wt% of $H_2O$ added to the starting composition) at 0.5–2.5 GPa and 900–1220 °C. These experiments provide context for the predominantly low-pressure experiments (conducted at ≤0.5 GPa) that are the principal subject of this present study. L1 was described in detail by Ewart et al. (1973). It is a porphyritic ba-saltic andesite lava containing ~27% phenocrysts that include: $An_{94}$ plagioclase (24%), augite and pigeonite (2%), orthopyroxene (0.3%), and magnetite (0.1%). The matrix comprises 67% glass together with microcrystalline plagioclase and clinopyroxene. L1 was chosen as the starting material as it was one of the most primary composi-tions available (truly 'primitive' compositions have not been recov-ered from the Tonga arc) and was also the the most crystal-poor sample from Late that contains all three pyroxene phases. Mineral compositions from L1 are reported by Ewart et al. (1973). For further comparison, mineral analyses were performed on a second, compa-rable sample from Late (L2). Both sets of data are reported in Table 1. On the basis of textural and mineral chemistry data, Ewart et al. (1973) inferred that crystallisation took place at ~1165–1216 °C and ≤0.1 GPa. Oxygen fugacity has not been determined for volca-nic rocks from Late, however Caulfield et al. (2012) estimated $fO_2$ for basaltic andesites from Tofua to be 1–1.2 log units above the quartz-fayalite-magnetite buffer (~Ni-NiO + 0.5).

The starting material was prepared by fusing a 2 g powdered sample of L1 for one hour in a 1 atm vertical furnace at 1200 °C. After being quenched in water the resulting glass was re-ground and the combined process repeated another two times to ensure complete melting and glass homogeneity. The final powder was dried at 120 °C and examined with a petrographic microscope to confirm that it was crystal free. Back-scattered electron images of the experimental run products taken after the experiments also showed no inherited crystals. Three different ex-perimental apparatus were employed for the experiments, dependent on the pressure required. These included:

Table 1
Composition of starting material L1.

| | L1 Whole rock | L1 Groundmass | L1 Glass | L2 | L1 Pl | L2 Pl | L1 Cpx | L1 Pig | L2 Pig | L2 Pig |
|---|---|---|---|---|---|---|---|---|---|---|
| Source | Ewart et al. (1973) | Ewart et al. (1973) | Green et al. (1989) | Ewart et al. (1973) | Ewart et al. (1973) | This Study | Ewart et al. (1973) | Ewart et al. (1973) | This study | This study |
| n | – | – | | – | – | 10 | – | – | 12 | 12 |
| Analysis location | – | – | | – | – | ANU | – | – | ANU | MQGA |
| $SiO_2$ | 55.05 | 56.56 | 54.09 | 53.66 | | 48.03 | 52.48 | 53.39 | 53.44 | 53.45 |
| $TiO_2$ | 0.57 | 0.83 | 0.56 | 0.51 | | 0.02 | 0.23 | 0.15 | 0.14 | 0.15 |
| $Al_2O_3$ | 17.53 | 14.19 | 17.76 | 15.45 | | 33.12 | 2.05 | 1.48 | 1.03 | 1.09 |
| $FeO_T$ | 9.35 | 12.46 | 9.82 | 9.90 | 1.03 | 1.16 | 10.27 | 16.92 | 17.71 | 17.72 |
| MnO | 0.19 | 0.21 | 0.19 | 0.19 | | 0.01 | 0.28 | 0.4 | 0.44 | 0.44 |
| MgO | 4.20 | 3.71 | 4.02 | 6.29 | 0.23 | 0.17 | 16.54 | 24.34 | 23.32 | 23.19 |
| CaO | 10.93 | 9.27 | 11.14 | 11.18 | 17.03 | 16.35 | 18.56 | 3.51 | 4.81 | 4.90 |
| $Na_2O$ | 1.78 | 1.97 | 1.78 | 1.49 | 1.82 | 1.78 | | | 0.04 | 0.04 |
| $K_2O$ | 0.40 | 0.69 | 0.56 | 0.39 | 0.06 | 0.07 | | | 0.01 | 0.02 |

1. piston-cylinder apparatus (for experiments at 0.5 to 2.5 GPa);
2. internally-heated pressure vessels (for 0.2 GPa experiments); and
3. vertical muffle-tube furnaces with controlled oxygen fugacities (for 1 atm experiments).

All starting materials other than those used in the 1 atm experiments were contained in sealed metal capsules made of Pt, Au, $Ag_{70}Pd_{30}$, $Ag_{50}Pd_{50}$ or $Au_{90}Pd_{10}$ dependent on run temperatures and the facility where experiments were conducted (Table 2). For water-bearing ex-periments, capsules were first loaded with 2 to 9.5 wt% of deionized $H_2O$ using a graduated micro-syringe (Table 2) and then filled with the powdered starting glass. To avoid $H_2O$ loss during the sealing of cap-sules, capsules were partially wrapped in wet tissue paper while being welded. After welding, capsules were first dried and then weighed. The integrity of capsules against water loss was then tested by placing them in an oven at 120 °C (for at least 10 min) before re-weighing.

The piston-cylinder experiments were conducted at Macquarie Uni-versity (Sydney, Australia) using an end-loaded piston-cylinder appara-tus of the type described by Boyd and England (1960). They were performed using a cold piston-in technique with furnace assemblies of 12.7 mm diameter, talc outer-sleeves and pyrex® inner-sleeves. Inter-nal components were made of air-fired boron nitride. A − 10% correc-tion was made to measured pressures for the effects of friction by the talc furnace assemblies (Green et al., 1966). Oxygen fugacities were not buffered but are estimated to have been between the Ni-NiO and magnetite-wüstite buffers (Green, 1976). Temperatures were moni-tored using either chrome-alumel (for older experiments at b1160 °C) or S-type ($Pt-Pt_{90}Rh_{10}$) thermocouples and automatically controlled by either a Leeds & Northrup Electromax V single-loop controller or a mercury-relay switch (the latter applied to the older experiments com-prised by runs 15–60). Run durations varied from 1 to 28 h. At the end of each run experiments were isobarically quenched by turning off the power to furnace assemblies.

All of the 0.2 GPa experiments were performed in internally heated pressure vessels at the Institut des Sciences de la Terre d'Orléans (ISTO-CNRS), France. Up to 5 individual charges were loaded at a time. Oxygen fugacity ($fO_2$) was controlled by loading ~1.1 or 6 bar of $H_2$ into the ves-sels. These impose $fO_2$ of ~Ni-NiO + 1 and FMQ respectively (Table 2). Experimental pressure and temperature were then attained by loading Ar into the vessel, followed by heating at a rate of 10–15 °C/min. The ex-periments were run for ~87 h at the lowest temperature (950 °C) and for ~48 h at the highest temperature (1070 °C). All experiments were terminated by drop quenching. Temperature and total pressure were continuously monitored; their uncertainties are ±5 °C and ± 2 MPa respectively.

One-atmosphere (1-atm) experiments were performed at the Re-search School of Earth Sciences, The Australian National University, Can-berra. Aliquots of the powdered glass starting material (L1) were mixed with polyethylene oxide reagent to form a paste, which was mounted onto loops made from 0.25 mm diameter palladium wire, to form beads of 3–5 mm diameter when melted. The samples were run in a ver-tical muffle tube furnace equipped for gas-mixing, with two samples run adjacent to each other at each temperature interval. Palladium was used in place of the more usual platinum to stop loss of iron from alloying with the metal loop, a well-known problem with Pt loops that becomes negligible with Pd under the relatively high oxygen fugac-ities of these experiments. These oxygen fugacities were imposed by the upward flow of a CO and $CO_2$ gas mixture (10,000 SCCM $CO_2$ to 100

Table 2
Experimental conditions and phase relationships.

| Experiment | P (GPa) | T (°C) | $H_2O$ (wt%) | $fO_2$ | Run duration (hrs) | Capsule type $Ag_{70}Pd_{30}$ | Thermocouple | Phases present[a] |
|---|---|---|---|---|---|---|---|---|
| 48 | 2.5 | 1220 | 5.0 | | 1 | | Cr-alumel | Liq |
| 43 | 2.5 | 1200 | 5.0 | | 1 | Pt | Type S | Liq + Gt + Cpx |
| 41 | 2.5 | 1160 | 5.0 | | 1 | Pt | Type S | Liq + Gt + Cpx |
| 29 | 2.5 | 1140 | 5.0 | | 4 | $Ag_{70}Pd_{30}$ | Cr-alumel | Liq + Gt + Cpx |
| 33 | 2.5 | 1100 | 5.0 | | 4 | $Ag_{70}Pd_{30}$ | Cr-alumel | Liq + Gt + Cpx |
| 39 | 2.5 | 1000 | 5.0 | | 9 | $Ag_{70}Pd_{30}$ | Cr-alumel | Liq + Gt + Cpx |
| 50 | 2.5 | 940 | 5.0 | | 20 | $Ag_{70}Pd_{30}$ | Cr-alumel | Liq + Gt + Cpx |
| 42 | 2.0 | 1140 | 5.0 | | 1.5 | Pt | Type S | Liq + Gt + Cpx |
| 15 | 2.0 | 1100 | 5.0 | | 4 | $Ag_{70}Pd_{30}$ | Cr-alumel | Liq + Gt + Cpx |
| 37 | 2.0 | 1040 | 5.0 | | 6 | $Ag_{70}Pd_{30}$ | Cr-alumel | Liq + Gt + Cpx |
| 35 | 2.0 | 940 | 5.0 | | 10.5 | $Ag_{70}Pd_{30}$ | Cr-alumel | Liq + Gt + Cpx |
| 28 | 1.5 | 1060 | 5.0 | | 6 | Pt | Type S | Liq + Gt + Cpx |
| 60 | 1.5 | 900 | 5.0 | | 27 | $Ag_{70}Pd_{30}$ | Cr-alumel | Liq + Gt + Cpx |
| 27 | 1.0 | 1020 | 5.0 | | 5 | $Ag_{70}Pd_{30}$ | Cr-alumel | Liq + Cpx |
| 31 | 1.0 | 980 | 5.0 | | 10 | $Ag_{70}Pd_{30}$ | Cr-alumel | Liq + Cpx |
| 32 | 1.0 | 940 | 5.0 | | 12 | $Ag_{70}Pd_{30}$ | Cr-alumel | Liq + Gt + Cpx |
| 40 | 1.0 | 900 | 5.0 | | 28 | $Ag_{70}Pd_{30}$ | Cr-alumel | Liq + Gt + Cpx |
| 36 | 0.5 | 1020 | 5.0 | | 8 | $Ag_{70}Pd_{30}$ | Cr-alumel | Liq |
| 34 | 0.5 | 980 | 5.0 | | 10 | $Ag_{70}Pd_{30}$ | Cr-alumel | Liq + Cpx |
| 47 | 0.5 | 900 | 5.0 | | 26 | $Ag_{70}Pd_{30}$ | Cr-alumel | Liq + Cpx + Opx + Pl |
| TR-9 | 0.2 | 1070 | 3.0 | NNO +1 | 48 | $Au_{90}Pd_{10}$ | Type S | Liq + Cpx + Pig + Pl |
| TR-2 | 0.2 | 1070 | 5.0 | NNO +1 | 48 | $Au_{90}Pd_{10}$ | Type S | Liq + Cpx + Pig + Pl |
| TR-16 | 0.2 | 1040 | 5.0 | NNO +1 | 53 | Au | Type S | Liq + Cpx + Pig + Pl |
| TR-17 | 0.2 | 1040 | 2.0 | NNO +1 | 53 | Au | Type S | Liq + Cpx + Pl |
| TR-22 | 0.2 | 1000 | 2.0 | NNO +1 | 61 | Au | Type S | Liq + Cpx + Opx + Pl + Sp |
| TR-11 | 0.2 | 1000 | 3.2 | NNO +1 | 61 | Au | Type S | Liq + Cpx + Opx + Pl + Sp |
| TR-4 | 0.2 | 1000 | 5.0 | NNO +1 | 61 | Au | Type S | Liq + Cpx + Pig + Pl + Sp |
| TR-21 | 0.2 | 1000 | 5.5 | NNO +1 | 61 | Au | Type S | Liq + Cpx + Pl + Sp |
| TR-20 | 0.2 | 1000 | 9.5 | NNO +1 | 61 | Au | Type S | Liq + Cpx + Pl + Sp |
| TR-10 | 0.2 | 985 | 5.0 | FMQ | 63 | Au | Type S | Liq + Cpx + Pl |
| TR-14 | 0.2 | 950 | 2.9 | NNO +1 | 87 | Au | Type S | Liq + Cpx + Pl + Sp |
| TR-3 | 0.2 | 950 | 5.0 | NNO +1 | 87 | Au | Type S | Liq + Cpx + Pl + Sp |
| B16–12 | 1 atm | 1242 | 0.0 | NNO + 0.85 | 21 | Pd wire | Type B | Liq |
| B02–12 | 1 atm | 1196 | 0.0 | NNO + 0.74 | 115 | Pd wire | Type B | Liq + Pl |
| B26–12 | 1 atm | 1177 | 0.0 | NNO + 0.7 | 88 | Pd wire | Type B | Liq + Pl |
| B17–12 | 1 atm | 1158 | 0.0 | NNO + 0.65 | 63 | Pd wire | Type B | Liq + Pl |
| B22–12 | 1 atm | 1139 | 0.0 | NNO + 0.61 | 91 | Pd wire | Type B | Liq + Pig + Pl |
| B29–12 | 1 atm | 1120 | 0.0 | NNO + 0.56 | 67 | Pd wire | Type B | Liq + Pig + Pl |

[a] Liq = Liqid; Gt = Garnet; Cpx = Clinopyroxene; Pig = Pigeonite; Opx = Orthopyroxene; Pl = Plagioclase; Sp = Spinel

SCCM; 99.0% $CO_2$) regulated by Tylan F2800 mass flow controllers. This gas mix produces oxygen fugacities that vary from 0.56 log units above the Ni-NiO buffer at 1120 °C to 0.85 log units above Ni-NiO at 1242 °C (O'Neill and Pownceby, 1993), with uncertainties estimated to be ± 0.05 log units. The samples were loaded into the furnace at ~600 °C, which is sufficiently low a temperature to prevent the loops from stick-ing to the sides of the muffle tube or to each other. Once samples were loaded, the flow of CO and $CO_2$ gases was commenced and the temper-ature increased at 6 °C/min to the final run temperature. The tempera-ture of the furnace was controlled from a type B thermocouple ($Pt_{94}Rh_6$-$Pt_{70}Rh_{30}$) external to the muffle tube, and thus not exposed to the CO-$CO_2$ gas mixture, and measured with a second type B thermo-couple positioned directly above the samples. The difference between the two thermocouples (generally 10 to 15 °C) did not vary during the run; this provides evidence against poisoning of the measuring thermo-couple, which is anyway not expected with the gas mixture used. Other thermocouples made from the same spool of wire as the measuring thermocouple were checked against the melting point of gold and found to be within ±1 °C of the 1064.2 °C fixed point of the ITS90 tem-perature scale. Reported temperatures are estimated to be accurate rel-ative to this scale to ±2 °C. All samples except one were run for 48 h (Table 2). At the conclusion of experiments samples were quenched by dropping into water.

The products from all experiments were mounted in epoxy and polished before being visually inspected with a reflected light micro-scope. The phases present in each experiment were initially identified using a Zeiss EVO MA15 scanning electron microscope with an Oxford Instruments Aztec Synergy EDS system. Mineral and glass chemistry was subsequently analysed in thirteen experiments by wavelength dis-persive spectrometers (WDS) using Cameca SX100 instruments at both the Australian National University (ANU), Canberra, and the Macquarie Geoanalytical laboratories, Macquarie University, Sydney. Mineral anal-yses were achieved using a 1 μm diameter beam, while a defocused 10 μm diameter beam was used for glass analyses in order to reduce Na-loss. A beam current of 10 nA and voltage of 15 kV was used. Analyses of Smithsonian Microbeam Standards RVM Garnet (NMNH87375), Kakanui Augite (NMNH122142) and Basaltic Glass VG-2 (NMNH 111240–52) were used to assess accuracy and precision at ANU, while the glass standards KL2-G, BHVO-2G and V99-G were used at Macquarie University. All analyses were within ±5% (relative) of recommended values. Phenocrysts from sample L2 (Table 1) were also analysed at both institutions to assess relative accuracy (b0.13 wt%) as well as to provide comparisons between the natural rock and experimental run products.

As a further check on the representativeness and accuracy of phase compositions, mass balances were calculated between the major ele-ment concentrations of run products and starting materials. This pro-vided estimates of run product modes while also allowing Fe and Na loss to be quantitatively assessed for individual experiments. For exper-iments conducted at ≤0.5 GPa $\Sigma r^2$ is always b0.3 (Table 3 – Online only). However, for a number of experiments where limited areas of glass ne-cessitated the use of a focused (1 μm) beam during EMP analyses, some Na loss is evident. For these cases original Na concentrations were esti-mated from mass balances. These values are presented in Table 3 (On-line only) together with the originally analysed $Na_2O$ concentrations.

## 3. Results

A list of the run products from each experiment is presented in Table 2. Liquidus phase equilibria interpreted for the basaltic andesite with 5 wt% of $H_2O$ are shown in Fig. 3. All of the experiments produced glasses with 36 out of 38 experiments crystallising at least one mineral phase. Some of the glasses from the 0.2 GPa experiments are vesicular. This is most evident for experiments with ≥5 wt% $H_2O$. Where present, garnet forms equant, euhedral crystals 1–50 μm in diameter. Pyroxenes typically occur as small (b 20 μm in diameter) euhedral grains, but in a number of experiments (e.g. run 41) they form accumulations of fine lath-like crystals with an interlocking texture. The plagioclase from 1 atm experiments forms radiating sheaths of filamentous crystals, whereas in hydrous experiments at 0.2–0.5 GPa it appears as tabular crystals of relatively equant form.

The minimum liquidus temperature (~1000 °C) for the bulk compo-sition with 5 wt% of $H_2O$ is encountered at ~0.5 GPa (Fig. 3). For this composition, augite is the sole liquidus phase at N0.2 to ~2.0 GPa. This is joined by pigeonite and plagioclase at 0.2 GPa and by garnet at 2.5 GPa. But at 1 atm and between 1200 and 1240 °C plagioclase is the only liquidus phase with pigeonite restricted to sub-liquidus conditions of ≤1158 °C. For experiments at 0.2 GPa with $H_2O$ concentrations either higher or lower than 5 wt%, sub-liquidus assemblages are similar to those for experiments with 5 wt% $H_2O$ except that pigeonite is replaced by orthopyroxene at 1000 °C in experiments with 2.0 and 3.2 wt% $H_2O$ (Table 2). No low-Ca pyroxenes were produced in any of the 0.2 GPa ex-periments at b1000 °C. Spinel appears in experiments with 5 wt% $H_2O$ at pressures b0.5 GPa and temperatures b1000 °C.

The major and minor element compositions of glasses and minerals from selected experiments are presented in Table 3 (Online only). Com-positional relations for the pyroxenes and plagioclases are shown in Figs. 4 and 5. Relations for melts (glasses) are plotted in Figs. 6 and 7. All pyroxenes produced at ≥1.0 GPa are augites with compositions in the range $Wo_{21\text{-}37}En_{45\text{-}58}Fs_{14–24}$. Wo content typically decreases with increasing pressure and temperature, whereas En, Fs and Jd contents increase. The analysed 0.5 GPa experiment produced augite ($Wo_{23\text{-}25}En_{42\text{-}44}Fs_{33}$), pigeonite ($Wo_{17}En_{45}Fs_{38}$) and enstatite ($Wo_{0\text{-}2}En_{52\text{-}56}Fs_{43–46}$). Pigeonite ($Wo_{6\text{-}15}En_{60\text{-}69}Fs_{25–30}$) is the sole pyroxene produced by the 1 atm experiments. The plagioclase from all experiments is calcic ($An_{74.0–91.1}$) but becomes more sodic with increas-ing pressure and degree of crystallisation. Conversely, it becomes more calcic with increasing $H_2O$ and decreasing temperature for a constant de-gree of crystallisation (Fig. 5a). All analysed garnets have similar compo-sitions, with 37–40% almandine, 28–36% grossular and 22–30% pyrope. The lowest pyrope and highest grossular contents are from the lowest temperature sample analysed (940 °C). The spinel from 0.2 GPa experi-ments is of predominantly magnetite composition with relatively low Cr (1.25 wt% $Cr_2O_3$) but significant proportions of the spinel-hercynite (~20 mol%) and ulvospinel (~13 mol%) components. The glasses pro-duced in experiments are mostly of andesite to dacite composition. They become increasingly more evolved as crystallisation progresses, but also vary with pressure and melt $H_2O$ concentration (Figs. 6 and 7).

The estimated Fe-loss from most experiments was too small to be certain of (i.e. b 1 wt%), however some of the older experiments (con-ducted at ≥1.5 GPa in Pt capsules) experienced significant Fe loss, amounting to 20–30% of the original Fe in the starting materials.

## 4. Discussion

### 4.1. Approach to equilibrium during experiments

All our experiments were synthesis experiments and no attempt was made at reversals. A number of features suggest, however, that equilibrium was sufficiently well approached for the experiments to provide a reliable guide to equilibria in the natural basaltic andesite magma. These include:

1. homogenous glasses;
2. euhedral crystal shapes; and
3. regular variations in the proportions, compositions and identities of phases as functions of pressure, temperature and $H_2O$ content.

Minor inconsistencies in the CaO concentrations of pyroxenes pro-duced at low temperatures (b1000 °C) and during short duration (b24 h) experiments (Table 3 – Online only) indicate a degree of meta-stability during some runs. This may account for the non-appearance of

Table 3
Mass balance and phase chemistry for 13 selected experimental runs.

| | P (GPa) | T (°C) | $H_2O$ (wt %) | $\Sigma R^2$ | Mass balance fraction | Phase | n | $SiO_2$ | $TiO_2$ | $Al_2O_3$ | FeO | MnO | MgO | CaO | $Na_2O$ | $K_2O$ | $P_2O_5$ | $Cr_2O_3$ | NiO | Sum |
|---|---|---|---|---|---|---|---|---|---|---|---|---|---|---|---|---|---|---|---|---|
| Run 35 | 2 | 940 | 5 | 1.267 | 0.13 | Clinopyroxene | 9 | 53.60 | 0.27 | 9.66 | 6.24 | 0.06 | 9.94 | 18.88 | 1.22 | 0.08 | 0.02 | 0.02 | 0.01 | 100.00 |
| | | | | | | ± | | 1.01 | 0.04 | 0.51 | 0.47 | 0.01 | 0.35 | 0.65 | 0.04 | 0.04 | 0.02 | 0.02 | 0.02 | |
| | | | | | 0.43 | Garnet | 11 | 40.39 | 1.16 | 19.62 | 19.99 | 0.43 | 5.45 | 12.75 | 0.05 | 0.01 | 0.13 | 0.01 | 0.01 | 100.00 |
| | | | | | | ± | | 0.65 | 0.29 | 0.52 | 2.03 | 0.10 | 0.66 | 0.82 | 0.04 | 0.01 | 0.05 | 0.01 | 0.01 | |
| | | | | | | Glass (measured) | 2 | 72.03 | 0.17 | 15.87 | 1.75 | 0.01 | 0.91 | 6.07 | 2.12 | 1.01 | 0.05 | 0.00 | 0.01 | 100.01 |
| | | | | | 0.40 | Glass (calculated) | | 71.55 | 0.17 | 15.76 | 1.74 | 0.01 | 0.91 | 6.03 | 2.78 | 1.00 | 0.05 | 0.00 | | 100.00 |
| | | | | | | ± | | 0.05 | 0.02 | 0.14 | 0.08 | 0.02 | 0.16 | 0.29 | 0.26 | 0.04 | 0.00 | 0.00 | 0.01 | |
| Run 37 | 2 | 1040 | 5 | 0.47 | 0.15 | Clinopyroxene | 6 | 51.35 | 0.26 | 9.73 | 7.73 | 0.08 | 10.42 | 19.22 | 1.09 | 0.08 | 0.02 | 0.02 | 0.02 | 100.00 |
| | | | | | | ± | | 0.55 | 0.05 | 0.58 | 0.46 | 0.01 | 0.46 | 0.67 | 0.06 | 0.05 | 0.02 | 0.01 | 0.02 | |
| | | | | | 0.32 | Garnet | 15 | 37.88 | 1.21 | 21.41 | 20.67 | 0.52 | 6.21 | 11.94 | 0.04 | 0.01 | 0.12 | 0.01 | 0.01 | 100.00 |
| | | | | | | ± | | 0.27 | 0.22 | 0.32 | 0.86 | 0.05 | 0.32 | 0.43 | 0.02 | 0.01 | 0.03 | 0.01 | 0.01 | |
| | | | | | 0.48 | Glass | 13 | 67.62 | 0.36 | 16.88 | 3.72 | 0.04 | 0.99 | 7.42 | 1.99 | 0.83 | 0.13 | 0.00 | 0.01 | 100.00 |
| | | | | | | ± | | 0.72 | 0.03 | 0.33 | 0.33 | 0.01 | 0.26 | 0.58 | 0.19 | 0.05 | 0.04 | 0.01 | 0.01 | |
| Run 15 | 2 | 1100 | 5 | 0.21 | 0.09 | Clinopyroxene | 4 | 51.63 | 0.29 | 8.06 | 8.50 | 0.12 | 10.87 | 19.75 | 0.72 | 0.03 | 0.01 | 0.02 | 0.01 | 100.00 |
| | | | | | | ± | | 0.14 | 0.04 | 0.38 | 0.13 | 0.02 | 0.16 | 0.21 | 0.03 | 0.01 | 0.01 | 0.02 | 0.01 | |
| | | | | | 0.19 | Garnet | 18 | 38.40 | 1.06 | 21.82 | 19.02 | 0.56 | 7.96 | 11.06 | 0.02 | 0.01 | 0.06 | 0.02 | 0.01 | 100.00 |
| | | | | | | ± | | 0.27 | 0.17 | 0.20 | 0.30 | 0.05 | 0.24 | 0.32 | 0.03 | 0.01 | 0.03 | 0.01 | 0.01 | |
| | | | | | 0.67 | Glass | 15 | 59.90 | 0.50 | 17.43 | 7.64 | 0.10 | 2.36 | 9.54 | 1.81 | 0.60 | 0.11 | 0.01 | 0.01 | 100.00 |
| | | | | | | ± | | 0.25 | 0.03 | 0.09 | 0.09 | 0.01 | 0.09 | 0.17 | 0.08 | 0.03 | 0.03 | 0.01 | 0.01 | |
| Run 42 | 2 | 1140 | 5 | 2.271 | 0.20 | Garnet | 13 | 38.73 | 1.14 | 21.34 | 18.86 | 0.55 | 7.46 | 11.76 | 0.06 | 0.01 | 0.06 | 0.02 | 0.01 | 100.00 |
| | | | | | | ± | | 0.56 | 0.22 | 0.68 | 1.38 | 0.02 | 1.21 | 0.44 | 0.07 | 0.01 | 0.04 | 0.01 | 0.01 | |
| | | | | | 0.05 | Pyroxene | 5 | 50.06 | 0.25 | 8.98 | 6.81 | 0.15 | 12.50 | 20.35 | 0.82 | 0.02 | 0.01 | 0.04 | 0.01 | 100.00 |
| | | | | | | ± | | 0.52 | 0.03 | 0.59 | 0.84 | 0.01 | 0.44 | 0.69 | 0.07 | 0.01 | 0.01 | 0.02 | 0.01 | |
| | | | | | 0.70 | Glass | 8 | 59.08 | 0.59 | 18.23 | 5.99 | 0.15 | 3.17 | 10.36 | 1.76 | 0.56 | 0.10 | 0.01 | 0.01 | 100.00 |
| | | | | | | ± | | 0.41 | 0.05 | 0.21 | 0.16 | 0.01 | 0.08 | 0.22 | 0.15 | 0.04 | 0.03 | 0.01 | 0.01 | |
| Run 27 | 1 | 1020 | 5 | 1.161 | 0.03 | Clinopyroxene | 11 | 49.29 | 0.43 | 6.56 | 9.29 | 0.21 | 13.14 | 20.43 | 0.34 | 0.01 | 0.21 | 0.08 | 0.02 | 100.00 |
| | | | | | | ± | | 0.73 | 0.08 | 0.76 | 0.54 | 0.02 | 0.48 | 0.34 | 0.03 | 0.01 | 0.03 | 0.02 | 0.02 | |
| | | | | | 0.92 | Glass | 10 | 55.89 | 0.60 | 17.25 | 9.38 | 0.17 | 3.97 | 10.31 | 1.81 | 0.52 | 0.10 | – | – | 100.00 |
| | | | | | | ± | | 0.19 | 0.03 | 0.19 | 0.09 | 0.03 | 0.05 | 0.08 | 0.04 | 0.01 | 0.02 | – | – | |
| Run 47 | 0.5 | 900 | 5 | 0.291 | 0.04 | Orthopyroxene | 6 | 50.10 | 0.32 | 3.06 | 26.15 | 0.45 | 17.91 | 1.94 | 0.01 | 0.01 | 0.02 | 0.02 | 0.01 | 100.00 |
| | | | | | | ± | | 0.44 | 0.04 | 0.71 | 0.79 | 0.03 | 0.40 | 0.18 | 0.01 | 0.01 | 0.02 | 0.01 | 0.00 | |
| | | | | | 0.26 | Clinopyroxene | 3 | 50.79 | 0.63 | 5.49 | 16.40 | 0.35 | 11.56 | 14.46 | 0.20 | 0.08 | 0.01 | 0.02 | 0.01 | 100.00 |
| | | | | | | ± | | 0.50 | 0.11 | 1.35 | 0.88 | 0.02 | 0.91 | 0.54 | 0.03 | 0.06 | 0.02 | 0.00 | 0.00 | |
| | | | | | 0.21 | Plagioclase | 2 | 48.08 | 0.10 | 32.89 | 1.35 | 0.03 | 0.16 | 15.85 | 1.41 | 0.09 | 0.01 | 0.00 | 0.01 | 100.00 |
| | | | | | | ± | | 0.10 | 0.01 | 0.39 | 0.45 | 0.01 | 0.08 | 0.23 | 0.01 | 0.02 | 0.01 | 0.01 | 0.02 | |
| | | | | | | Glass (measured) | 2 | 61.47 | 0.67 | 19.13 | 8.18 | 0.14 | 1.27 | 7.49 | 0.76 | 0.67 | 0.20 | 0.00 | 0.01 | 100.00 |
| | | | | | 0.45 | Glass (calculated) | | 60.87 | 0.66 | 18.94 | 8.10 | 0.14 | 1.25 | 7.42 | 1.75 | 0.67 | 0.20 | 0.00 | | 100.00 |
| | | | | | | ± | | 0.06 | 0.03 | 0.25 | 0.65 | 0.01 | 0.26 | 0.05 | 0.45 | 0.08 | 0.03 | 0.00 | 0.01 | |
| Run 36 | 0.5 | 1020 | 5 | – | – | Glass | 13 | 55.64 | 0.51 | 17.54 | 9.33 | 0.17 | 3.92 | 10.76 | 1.54 | 0.47 | 0.09 | 0.01 | 0.01 | 100.00 |
| | | | | | | ± | | 0.16 | 0.02 | 0.11 | 0.12 | 0.02 | 0.05 | 0.14 | 0.04 | 0.02 | 0.03 | 0.01 | 0.01 | |
| TR-3 | 0.2 | 950 | 5 | 0.96 | 0.17 | Clinopyroxene | 9 | 49.32 | 0.47 | 3.89 | 9.42 | 0.31 | 15.26 | 20.86 | 0.17 | 0.03 | 0.25 | 0.01 | 0.01 | 100.00 |
| | | | | | | ± | | 1.80 | 0.14 | 0.67 | 2.47 | 0.03 | 0.84 | 0.75 | 0.07 | 0.02 | 0.03 | 0.01 | 0.01 | |
| | | | | | 0.27 | Plagioclase | 9 | 45.98 | 0.03 | 32.94 | 1.52 | 0.02 | 0.16 | 17.89 | 1.18 | 0.05 | 0.22 | 0.00 | 0.01 | 100.00 |
| | | | | | | ± | | 1.05 | 0.02 | 0.80 | 0.32 | 0.02 | 0.16 | 0.55 | 0.14 | 0.03 | 0.02 | 0.01 | 0.01 | |
| | | | | | 0.05 | Fe-Ti Oxides | 7 | 0.75 | 4.92 | 3.98 | 87.41 | 0.31 | 2.05 | 0.44 | 0.03 | 0.01 | 0.01 | 0.06 | 0.03 | 100.00 |
| | | | | | | ± | | 0.56 | 0.09 | 0.12 | 0.76 | 0.02 | 0.07 | 0.07 | 0.02 | 0.01 | 0.02 | 0.01 | 0.03 | |
| | | | | | | Glass (measured) | 8 | 68.36 | 0.55 | 14.46 | 6.37 | 0.15 | 1.57 | 5.74 | 1.67 | 0.93 | 0.19 | – | – | 100.00 |
| | | | | | 0.46 | Glass (calculated) | | 67.99 | 0.55 | 14.39 | 6.33 | 0.15 | 1.57 | 5.70 | 2.21 | 0.93 | 0.19 | 0.00 | – | 100.00 |
| | | | | | | ± | | 0.48 | 0.08 | 0.34 | 0.48 | 0.02 | 0.19 | 0.23 | 0.21 | 0.14 | 0.02 | – | – | |
| TR-10 | 0.2 | 985 | 5 | 0.00 | 0.10 | Clinopyroxene | 9 | 50.63 | 0.38 | 4.07 | 9.63 | 0.24 | 14.52 | 20.26 | 0.15 | 0.04 | 0.04 | 0.03 | 0.01 | 100.00 |
| | | | | | | ± | | 0.49 | 0.09 | 1.11 | 0.58 | 0.03 | 0.69 | 0.72 | 0.03 | 0.03 | 0.02 | 0.02 | 0.01 | |
| | | | | | 0.10 | Plagioclase | 4 | 46.13 | 0.07 | 33.81 | 1.07 | 0.02 | 0.16 | 17.72 | 0.92 | 0.06 | 0.03 | 0.01 | 0.00 | 100.00 |
| | | | | | | ± | | 0.77 | 0.01 | 0.58 | 0.15 | 0.02 | 0.06 | 0.47 | 0.08 | 0.03 | 0.02 | 0.02 | 0.00 | |
| | | | | | 0.01 | Fe-Ti Oxide | 1 | 0.25 | 5.11 | 5.26 | 84.92 | 0.25 | 2.82 | 0.13 | 0.02 | 0.00 | 0.00 | 1.25 | 0.00 | 100.00 |
| | | | | | | Glass (measured) | 11 | 57.43 | 0.58 | 17.26 | 10.30 | 0.18 | 3.31 | 8.81 | 1.42 | 0.52 | 0.16 | 0.00 | | 99.99 |
| | | | | | 0.74 | Glass (calculated) | | 57.14 | 0.58 | 17.17 | 10.25 | 0.18 | 3.29 | 8.76 | 1.94 | 0.52 | 0.16 | 0.00 | 0.01 | 100.01 |
| | | | | | | ± | | 0.36 | 0.04 | 0.30 | 0.24 | 0.01 | 0.19 | 0.25 | 0.13 | 0.02 | 0.03 | 0.01 | 0.01 | |
| TR-4 | 0.2 | 1000 | 5 | 0.084 | 0.00 | Pigeonite | 7 | 53.18 | 0.14 | 1.00 | 17.48 | 0.42 | 23.00 | 4.61 | 0.05 | 0.00 | 0.04 | 0.04 | 0.02 | 100.00 |
| | | | | | | ± | | 0.47 | 0.03 | 0.03 | 0.38 | 0.03 | 0.38 | 0.21 | 0.01 | 0.00 | 0.02 | 0.02 | 0.02 | |
| | | | | | 0.13 | Clinopyroxene | 2 | 52.19 | 0.21 | 2.00 | 9.98 | 0.26 | 17.12 | 17.93 | 0.15 | 0.00 | 0.03 | 0.19 | 0.04 | 100.09 |
| | | | | | | ± | | 0.17 | 0.01 | 0.39 | 1.42 | 0.02 | 0.19 | 0.95 | 0.02 | 0.00 | 0.01 | 0.16 | 0.01 | |
| | | | | | 0.21 | Plagioclase | 18 | 47.52 | 0.03 | 32.94 | 1.13 | 0.01 | 0.14 | 16.53 | 1.62 | 0.05 | 0.01 | 0.01 | 0.01 | 100.00 |
| | | | | | | ± | | 0.89 | 0.02 | 0.73 | 0.10 | 0.01 | 0.05 | 0.52 | 0.31 | 0.02 | 0.01 | 0.01 | 0.01 | |
| | | | | | 0.02 | Fe-Ti Oxide | 1 | 0.25 | 5.11 | 5.26 | 84.92 | 0.25 | 2.82 | 0.13 | 0.02 | 0.00 | 0.00 | 1.25 | 0.00 | 100.00 |
| | | | | | | Glass (measured) | 4 | 59.83 | 0.74 | 15.91 | 10.73 | 0.19 | 3.10 | 7.70 | 0.94 | 0.68 | 0.16 | 0.01 | | 99.99 |
| | | | | | 0.60 | Glass (calculated) | | 59.38 | 0.74 | 15.79 | 10.65 | 0.18 | 3.08 | 7.64 | 1.69 | 0.67 | 0.16 | 0.00 | 0.01 | 100.01 |
| | | | | | | ± | | 0.48 | 0.03 | 0.24 | 0.07 | 0.01 | 0.13 | 0.23 | 0.17 | 0.01 | 0.05 | 0.02 | 0.01 | |
| TR-19 | 0.2 | 1040 | 0 | – | – | Glass | 12 | 55.36 | 0.54 | 17.41 | 9.79 | 0.18 | 3.81 | 10.58 | 1.70 | 0.52 | 0.09 | 0.01 | 0.01 | 100.00 |
| | | | | | | ± | | 0.18 | 0.02 | 0.14 | 0.06 | 0.01 | 0.04 | 0.10 | 0.09 | 0.03 | 0.04 | 0.01 | 0.01 | |
| B-29 | 1 atm | 1120 | 0 | 0.021 | 0.08 | Pigeonite | 10 | 52.39 | 0.24 | 2.29 | 16.39 | 0.44 | 21.34 | 6.49 | 0.06 | 0.01 | 0.01 | 0.22 | 0.13 | 100.00 |
| | | | | | | ± | | 0.36 | 0.04 | 0.70 | 0.96 | 0.03 | 1.07 | 1.36 | 0.04 | 0.02 | 0.02 | 0.04 | 0.02 | |
| | | | | | 0.33 | Plagioclase | 8 | 51.02 | 0.03 | 29.90 | 1.34 | 0.02 | 0.39 | 14.40 | 2.70 | 0.15 | 0.02 | 0.00 | 0.02 | 100.00 |
| | | | | | | ± | | 0.42 | 0.02 | 0.39 | 0.08 | 0.01 | 0.03 | 0.18 | 0.07 | 0.02 | 0.02 | 0.01 | 0.03 | |

(continued on next page)

Table 3 (continued)

| | P (GPa) | T (°C) | $H_2O$ (wt %) | $\Sigma R^2$ | Mass balance fraction | Phase | n | $SiO_2$ | $TiO_2$ | $Al_2O_3$ | FeO | MnO | MgO | CaO | $Na_2O$ | $K_2O$ | $P_2O_5$ | $Cr_2O_3$ | NiO | Sum |
|---|---|---|---|---|---|---|---|---|---|---|---|---|---|---|---|---|---|---|---|---|
| | | | | | 0.60 | Glass | 9 | 57.03 | 0.96 | 12.47 | 13.51 | 0.24 | 4.03 | 9.45 | 1.38 | 0.75 | 0.14 | 0.01 | 0.02 | 100.00 |
| | | | | | | ± | | 0.82 | 0.06 | 0.22 | 0.78 | 0.02 | 0.14 | 0.20 | 0.08 | 0.04 | 0.03 | 0.01 | 0.02 | |
| B-22 | 1 atm | 1139 | 0 | 0.30 | 4.00 | Pigeonite | 9 | 53.26 | 0.16 | 1.37 | 15.97 | 0.41 | 23.99 | 4.37 | 0.03 | 0.00 | 0.02 | 0.22 | 0.20 | 100.00 |
| | | | | | | ± | | 0.36 | 0.03 | 0.18 | 0.10 | 0.02 | 0.36 | 0.39 | 0.02 | 0.00 | 0.02 | 0.04 | 0.01 | |
| | | | | | 0.25 | Plagioclase | 15 | 50.77 | 0.04 | 30.00 | 1.51 | 0.01 | 0.42 | 14.55 | 2.55 | 0.12 | 0.02 | 0.01 | 0.01 | 100.00 |
| | | | | | | ± | | 0.55 | 0.02 | 0.34 | 0.18 | 0.02 | 0.08 | 0.31 | 0.15 | 0.01 | 0.02 | 0.01 | 0.01 | |
| | | | | | 0.75 | Glass | 11 | 55.46 | 0.78 | 13.16 | 12.86 | 0.24 | 5.63 | 9.72 | 1.38 | 0.60 | 0.12 | 0.01 | 0.02 | 100.00 |
| | | | | | | ± | | 0.47 | 0.03 | 0.14 | 0.24 | 0.02 | 0.24 | 0.18 | 0.06 | 0.04 | 0.03 | 0.01 | 0.02 | |

The calculated glass compositions are the same as measured values except for $Na_2O$ which has been corrected for loss during emp anayses. The $Na_2O$ values given are based on mass bal-ances between run products and starting compositions.
All values have been recalculated to total 100%.

low-Ca pyroxenes in experiments at b1000 °C and 0.2 GPa. Alterna-tively, given the low abundance of orthopyroxene in the natural rocks (b0.3%), small volumes of orthopyroxene may have inter-grown with more abundant clinopyroxene, making them difficult to distinguish in back-scattered images. Regardless, either scenario is unlikely to affect the validity of our final conclusions (see later discussion).

### 4.2. Conditions of basaltic andesite crystallisation and the production of Tongan dacite magmas

The two primary goals of our experiments were to determine:

a) the physical conditions of phenocryst precipitation from L1; and
b) whether crystal fractionation under the same or related conditions can account for the compositions of associated dacites.

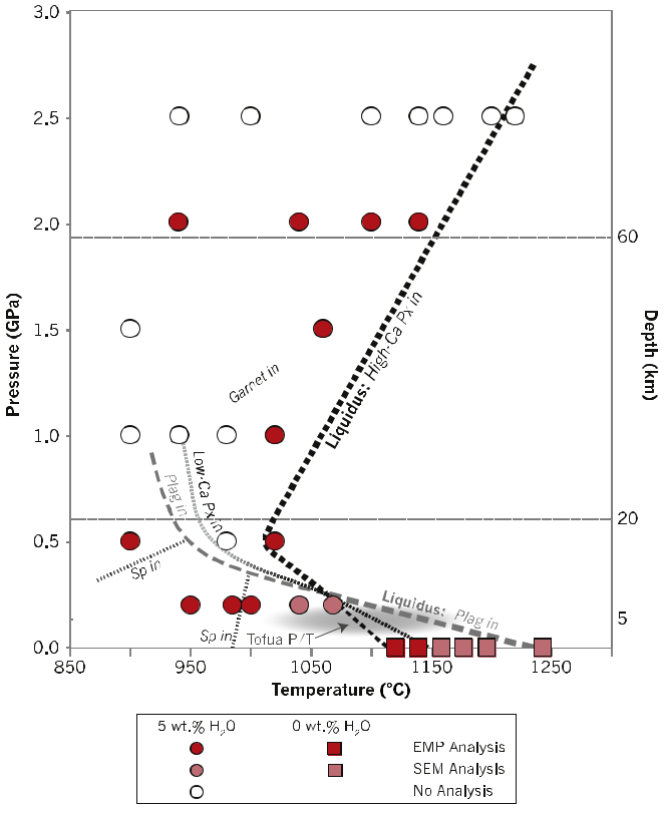


Fig. 3. Liquidus and sub-liquidus relations for the basaltic andesite L1 at 1 atm to 2.5 GPa with 5 wt% of $H_2O$ added to the starting composition. Note that at 1 atm experiments are effectively anhydrous although inferred to be $H_2O$-saturated at b0.5 GPa. P/T conditions inferred for crystallisation of basaltic andesites at Tofua (Caulfield et al., 2012) are shown for comparison. The shift in colour along the low-Ca pyroxene in cotectic reflects the transition between pigeonite (black) and orthopyroxene (grey), with pigeonite favouring higher temperatures and lower pressures.

The answer to the first question, related to conditions of phenocryst precipitation, is constrained by the experimentally determined liquidus relations of L1 with 5 wt% of added $H_2O$ (Fig. 3). These show that at ~0.2 GPa and 1100 °C, the liquidus of L1 is either at or close to multiple saturation with an aqueous fluid phase, and three of the rock's four phe-nocryst phases (plagioclase, pigeonite and augite). The presence of an aqueous fluid phase can be deduced from the ~100 °C depression of the liquidus at 0.5 GPa (Fig. 3), solubility data for $H_2O$ in andesitic melts (e.g. Botcharnikov et al., 2015), and the production of vesicular glasses in experiments at 0.2 GPa with ≥5 wt% of added $H_2O$.

The oxygen fugacity of the 0.2 GPa and 1 atm experiments (Ni-NiO + 0.56–1) is comparable with that estimated for Tongan magmas by Caulfield et al. (2012) (~Ni-NiO + 0.5). Using the conditions of experi-ment B16–12 (1242 °C; Ni-NiO + 0.85: Table 2) $Fe^{3+}/\Sigma Fe$ of 0.13 was calculated for the L1 starting material using the procedure of O'Neill et al. (2018). This method relies on magma composition, temperature and $fO_2$ and the low estimated $Fe^{3+}$, relative to $fO_2$, is a product of the low abundance of alkalis and CaO, but high $SiO_2$ in L1 when compared with MORB. Changes in $fO_2$ have only a limited effect on $Fe^{3+}/\Sigma Fe$ under these conditions. Thus dropping $fO_2$ by 1.5 log units (to QFM) de-creases $Fe^{3+}/\Sigma Fe$ only to 0.06. Clinopyroxene should have $Fe^{3+}/\Sigma Fe$ values either similar to or higher than the melt, so its stability should be relatively insensitive to likely differences between experimental and natural $fO_2$.

Orthopyroxene is observed as a minor phenocryst phase in L1 (0.3% by volume), but was not found in the experiments. As mentioned ear-lier, a low abundance in run products may have prevented its identifica-tion. Alternatively, as the coexistence of all three pyroxenes is only possible over a very limited range of temperature and pressure (see Lindsley and Andersen, 1983), the exact conditions required may fall into the gaps in our experimental coverage. In either case, additional constraints make it likely that the experimentally defined conditions of multiple-saturation (~0.2 GPa and 1100 °C) are comparable to those of phenocryst growth and magma evolution, even though orthopyro-xene was not precipitated. The first is the compositional similarity of the near-liquidus phases crystallised in the 0.2 GPa experiments to the phenocrysts in L1 (Figs. 4 and 5). In the case of plagioclase, the pheno-crysts ($An_{83.6}$) are most closely matched by the plagioclase from run TR4 ($An_{84.6}$) at 0.2 GPa and 1000 °C, with 5 wt% of $H_2O$ (Fig. 5a). A sim-ilar relationship occurs for augite with concentrations of Wo, En, Fs and $Al_2O_3$ in phenocrysts being most closely matched by the pyroxenes from near-liquidus experiments at 0.2 GPa (Figs. 4 and 5a; Table 3 – On-line only). Putirka's (2008) plagioclase-liquid hygrometer estimates a water content of 5 wt% using the plagioclase and glass compositions of the of the natural rock (Table 1) and a temperature of 1000 °C, consis-tent with run TR4.

A comparatively low pressure (~0.2 GPa) and $H_2O$-saturated origin for the phenocrysts in L1 is independently supported by $H_2O$ concentra-tions in melt inclusions hosted by phenocrysts in basaltic andesites on neighbouring Tofua. These inclusions contain up to 4.66 wt% $H_2O$ (Caulfield et al., 2012) but show an inverse relationship between $H_2O$ concentration and standard indices of melt fractionation. Thus

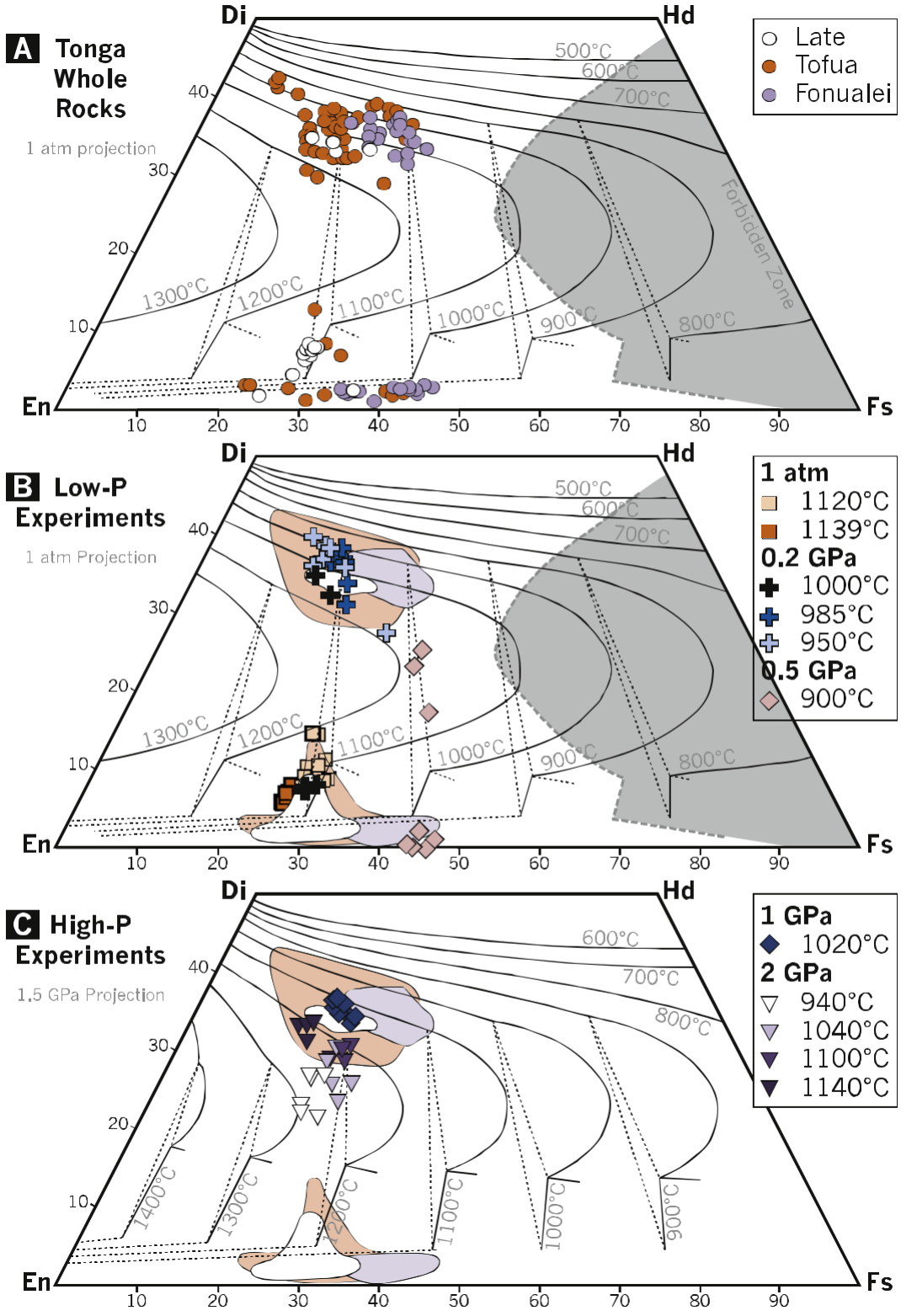


Fig. 4. Quadrilateral components in natural and experimentally-produced pyroxenes plotted using the projection scheme of Lindsley (1983). Because the relationships between coexisting pyroxenes are sensitive to pressure as well as temperature, the data for phenocrysts and low-pressure experiments on L1 (0.2 GPa and 1 atm) are projected against isotherms for 1 atm (Fig. 4a), whereas the data from higher pressure experiments (≥0.5 GPa) are projected against isotherms for 1.5 GPa (Fig. 4b). The experimental pyroxene compositions are from Table 3 (Online only). Data for pyroxene phenocrysts from L1 and other Tongan volcanics are from Ewart et al. (1973), Caulfield et al. (2012) and Turner et al. (2012). Fields showing natural phe-nocryst compositions from Late, Tofua and Fonualei are provided for comparison in panels b and c.

concentrations of $H_2O$ are highest in the most mafic inclusions and low-est in the most evolved. This relationship was interpreted by Caulfield et al. (2012) to be the result of melt evolution in response to $H_2O$ loss as melts depressurised during their ascent to the surface. In this case, solubility relationships for $H_2O$ in andesite magmas (e.g. Botcharnikov et al., 2015) confine magma evolution to pressures ≤0.16 GPa which is comparable to the experimentally determined conditions of multiple saturation for L1 + 5 wt% $H_2O$ (Fig. 3).

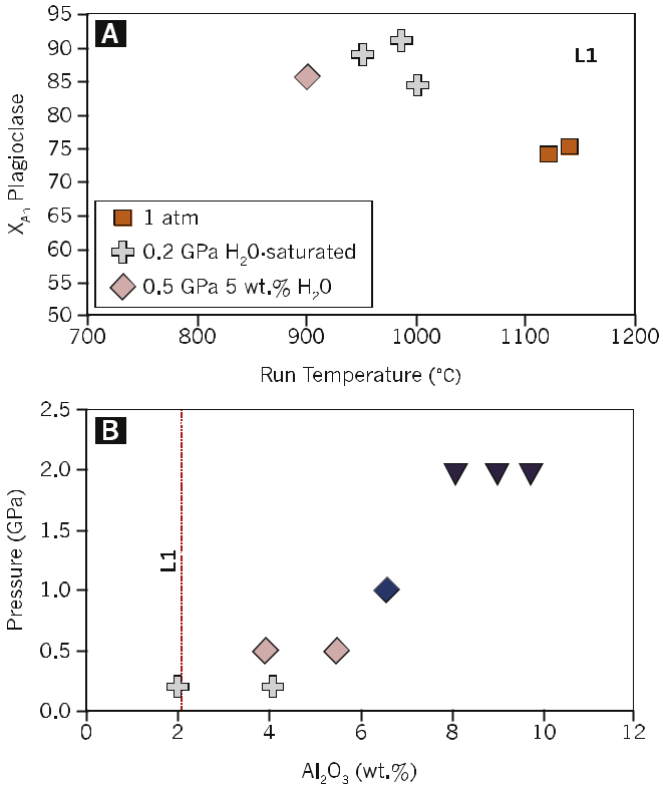


Fig. 5. (a) Variation in molecular AnX in experimentally produced plagioclase from L1 as a function of temperature. The bulk composition of plagioclase phenocrysts from L1 is shown in pink for comparison. The experimental data are from Table 3 (Online only) and the phenocryst composition from Ewart et al. (1973). (b) $Al_2O_3$ versus pressure of synthesis for augite experimentally crystallised from the basaltic andesite L1.

The liquidus relations of L1 reflect the broader controls exercised by pressure, temperature and $H_2O$ on cotectic relationships in multi-component compositional space. This is illustrated in Fig. 6 where the compositions of Tongan whole-rock and matrix samples are plotted for comparison with cotectic relations for plagioclase and two pyrox-enes at 1 atm, 0.2 GPa and 2.0 GPa. The latter were derived from the ex-perimental data for L1 (chiefly glass compositions) with all major and

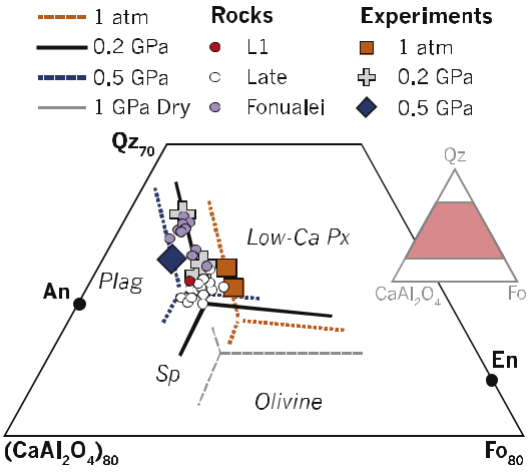


Fig. 6. Bulk rock compositions for Late and Fonualei projected within the pseudo-ternary $CaAl_2O_4$-silica-forsterite system using the scheme of O'Hara (1968). Plotted for comparison are cotectics for plagioclase and pyroxenes at 1 atm, 0.2 GPa ($H_2O$-saturated), and 0.5 GPa (with 5 wt% of $H_2O$ in the liquid phase). The plagioclase-pyroxene cotectics are based on experimental data from this study (Table 3 – Online Only). The natural rock compositions are from Ewart et al. (1973), Caulfield et al. (2012), Turner et al. (2012) and Beier et al. (2017).

minor element oxides recalculated as CMAS ($CaO$-$MgO$-$Al_2O_3$-$SiO_2$) components following the procedure of O'Hara (1968).

The whole-rock samples from Late, Fonualei and Tofua (including dacites) fall either on or near the $H_2O$-saturated 0.2 GPa cotectic for pla-gioclase, low-Ca pyroxene and diopside (Fig. 6). A number of the more evolved matrix samples plot closer to the 1 atm cotectic, however, con-sistent with ongoing melt evolution and $H_2O$ loss during the final ascent of magmas to the surface. It can also be noted that at pressures N0.2 GPa the plagioclase-pyroxene cotectic shifts to melt compositions that are more plagioclase rich than most of our natural samples.

4.3. Conditions of dacite formation and changes in Dy/Yb beneath the Tonga Arc

Most arc magmas are of andesite to basaltic andesite composition (see Adam et al., 2016). However, dacites may be locally dominant (as on Fonualei) and their origins are central to debates about the condi-tions and processes of arc crust evolution. For example, some workers (e.g. Annen et al., 2006) attribute dacite magma formation to repeated under-plating and melting at the base of the arc crust, while others sup-port an origin by crystal fractionation in the upper crust (e.g. Adam et al., 2016). The difficulty of discriminating between these processes is most acute in primitive, intra-oceanic arcs, like Tonga, where isotopic con-trasts between incoming magma from the mantle wedge and the over-lying crust are minimal. In such cases, identification of the minerals involved becomes crucial for correctly interpreting trace element trends (Brophy, 2008).

In the case of Tonga, our experiments lend support to the shallow crystal fractionation argument by demonstrating that dacite magmas can be produced by low pressure (≤ 0.2 GPa) fractionation involving the removal of plagioclase + augite ± pigeonite + titanomagnetite from hydrous basaltic andesite magmas. This was most closely achieved in Run TR3 at 0.2 GPa and 950 °C where most of the phenocryst phases (including plagioclase, clinopyroxene and spinel) present in the Fonualei dacites were also reproduced (Table 2). Furthermore, mineral and glass compositions are comparable between the Fonualei dacites and this experiment (Figs. 4 and 7). Rapid evolution to dacite, as in-ferred from time scale estimates (Turner et al., 2003), and magma-cumulate mixing, provide mechanisms for the production of dacites containing entrained antecrysts of $Fo_{92}$ olivine and $An_{85}$ plagioclase similar to those erupted at Metis Shoal (Ewart et al., 1973).

Our conclusions have implications for a related and topical debate concerning the role of amphibole in arc magma genesis (Davidson et al., 2007). This arises because the evolution to increasingly low Dy/ Yb in some arc suites is popularly attributed to the fractionation of am-phibole (which preferentially incorporates the middle over heavy rare earth elements) although many dacites with these characteristics do not contain amphibole (see Davidson et al., 2007). The 'cryptic' role that this implies for amphibole (e.g. Davidson et al., 2007, 2013) has the potential problem that amphibole is not normally a liquidus phase of the supposed parent magmas (andesites and basaltic andesites) and once present may not be removed from the crystallisation sequence by normal peritectic relationships (although see Smith, 2014; Blatter et al., 2017).

None of the experiments on L1 produced amphibole (Table 2) and there is no record of amphibole in any volcanic rock from the Tonga Arc (e.g. Ewart et al., 1973). Amphibole is commonly associated with crystallisation of hydrous magmas. The absence of amphibole among water-rich ($H_2O$ ~4–5 wt%) Tongan magmas shows that the lack of am-phibole does not necessarily imply water-poor conditions. Rather, the low-alkali content of island arc tholeiites reduces amphibole stability. Dacite genesis in Tonga can be related to crystal fractionation involving plagioclase and pyroxenes. In this case, the fractionation produced by these phases must be responsible for the positive relationship between
Dy/Dy* and Dy/Yb that characterise individual Tongan volcanoes [where Dy* = $Dy_N/(La^{4/13}{}_N + Yb^{9/13}{}_N)$ see Davidson et al., 2013] (Fig. 8).

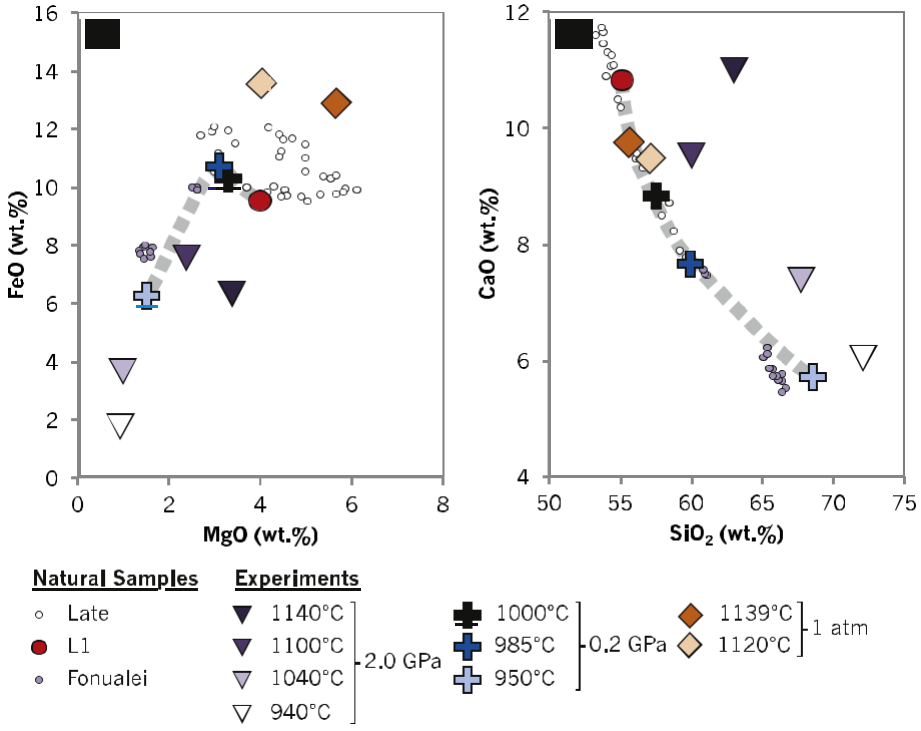


Fig. 7. Comparison of major element contents between natural samples from Late and Fonualei (Beier et al., 2017; Caulfield et al., 2012; Ewart et al., 1973; Turner et al., 2012) and experimental glasses. An inferred liquid line of descent for a hydrous (5 wt% $H_2O$) magma crystallising at 0.2 GPa has been shown, based on results of the 0.2 GPa experiments.

As the starting composition used in this study was not doped with trace elements, REE abundances in experimental products were below detec-tion limits for LA-ICPMS analysis. Instead, a modelling approach was used to explain the REE patterns observed in Tongan lavas. We employed a range of estimated D values (Table 4) for the partitioning of rare earth elements between pyroxenes and andesite-dacite melts (assuming negligible partitioning by plagioclase) and used them to calculate Dy/Dy* and Dy/Yb in melts produced by the progressive crystallisation of L1. The resulting liquid lines of descent are plotted in Fig. 8. These demonstrate that for Late, the positive relationship be-tween Dy/Dy* and Dy/Yb can be achieved by the fractionation of augite alone, without the involvement of amphibole. The situation may be dif-ferent for more hydrous, alkali-rich arc magmas. The effect of pigeonite and orthopyroxene on REE trends is less evident than that of augite, due to the very small absolute concentrations of rare earth elements that can be accommodated in these phases. Conversely, the compatibility of the heavy REE in garnet means that crystal fractionation of, or partial melt-ing in the presence of,this phase would lead to rapid increases in Dy/Yb. The absence of such effects in any of the Tongan lavas demonstrates that the magmas did not spend any time in the garnet stability field on Fig. 3. This provides further constraints on the P-T path traversed by the magmas.

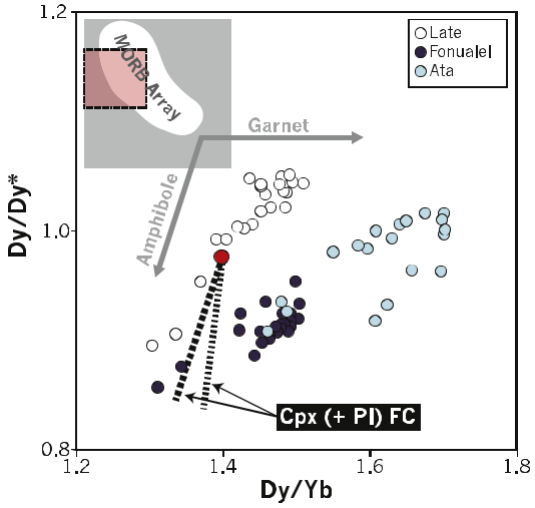


Fig. 8. Dy/Dy* versus Dy/Yb (see Davidson et al., 2013) for Tongan volcanoes. Heavy dashed lines represent two calculated liquid lines of descent produced by the fractionation of clinopyroxene and plagioclase from L1 (red circle). Both models consider the same frac-tionating assemblage (based on the modal abundance of phenocrysts in L1 – Ewart et al., 1973) but with differences in the partition coefficients assumed for Dy and Yb (Fujimaki et al., 1984; Wood and Blundy, 1997). As REE are highly incompatible in plagioclase, var-iations to the relative proportions of plagioclase and pyroxene in the fractionating assem-blage will influence the degree of fractionation along these vectors, but not their slope. Rare earth element concentrations in Tongan lavas are from Ewart et al. (1973); Caulfield et al. (2012); Turner et al. (2012); Beier et al. (2017). The inset in the top left shows the area shown in this figure relative to the MORB array.

### 4.4. Magmatic $H_2O$ and the development of the Tholeiitic trend in Arc Magmas

Subduction zones are most commonly associated with magmas of the calc-alkaline series (e.g. Gill, 1981). However tholeiitic arc magmas are also observed, most typically in arc-front volcanoes associated with the subduction of old and cold plates or with the early stages of arc vol-canism. They are less frequently encountered than their calc-alkaline counterparts but have been identified at a number of island arcs. These include the Tonga-Kermadec, Izu-Bonin-Mariana, Kurile and the western Bismark systems (Ewart et al., 1973; Gill, 1981; Hamada et al., 2014; Johnson et al., 1985).

Table 4
Clinopyroxene distribution coefficients used to model REE.

| Element | Fujimaki et al. (1984) | Wood and Blundy (1997) |
|---|---|---|
| La | 0.1047 | – |
| Dy | 0.6218 | 0.619 |
| Yb | 0.6010 | 0.552 |

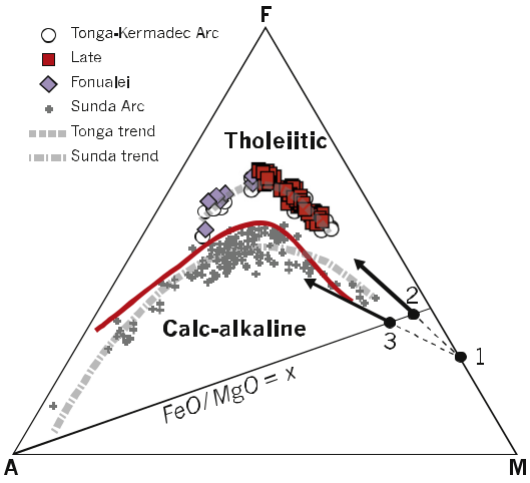


Fig. 9. AFM diagram illustrating the divergence of the tholeiitic trend of the Tonga-Kermadec Arc from the calc-alkaline trend of the Sunda Arc. Data for the Tonga-Kermadec Arc are from Ewart et al. (1973); Caulfield et al. (2012); Turner et al. (2012); Beier et al. (2017). Sunda Arc data is from the compilation of datasets used by Adam et al. (2016). The arrows show vectors for the melt compositions produced by crystal fractionation of olivine (1) and pyroxenes from two hypothetical parent magmas (2 and 3) with the same initial Fe/Mg but different alkali concentrations. It can be noted that alkali concentra-tions will increase more rapidly in melts derived from the more alkali-rich parent compo-sition (3). Conversely, the alkali-depleted parent composition (2) will fractionate more strongly toward Fe-enrichment and thus a tholeiitic trend.

As defined by Jakes and Gill (1970), tholeiites are distinguished by their pronounced iron-enrichments, low potassium concentrations and groundmass pigeonite. Island-arc tholeiites in particular, have been noted for their low total-alkali ($Na_2O + K_2O$) concentrations (e.g. Jakes and Gill, 1970; Kuno, 1959, 1968). The attributes of the calc-alkaline series are less easily defined (see Arculus, 2003) but when compared to tholeiites of similar $SiO_2$ content, calc-alkaline rocks display higher Al and lower Fe/Mg (Wilkinson, 1967). In the AFM (Total alkali/total iron/MgO) system (Fig. 9) they also show rela-tive alkali enrichments, whereas tholeiites of intermediate composition tend to high Fe. Although the debate over the causes of these differences has never been finalised, there is a consensus that calc-alkaline magmas are $H_2O$-rich (with ≥4 wt% $H_2O$) and that this plays a significant role in their evolution (e.g. Hamada and Fujii, 2008; Parman et al., 2011; Tatsumi and Suzuki, 2009; Zimmer et al., 2010).

The most common explanation for the association between high $H_2O$ concentrations and calc-alkaline magmas is that water delays pla-gioclase crystallisation in favour of Fe-bearing silicate minerals (e.g. ol-ivine and pyroxenes). This limits the enrichment of Fe in residual melts and thereby promotes a calc-alkaline fractionation trend. By default, the inverse argument might be expected to apply to tholeiitic arc magmas. However, while consistent with relationships for Al and total Fe, the in-fluence of water does not explain the high Fe/Mg versus $SiO_2$ that distin-guishes tholeiitic magmas. It is also inconsistent with the evidence for high $H_2O$ concentrations in tholeiitic magmas from Late and neighbouring Tongan volcanoes (2.34–4.66 wt% $H_2O$: Caulfield et al., 2012; Cooper et al., 2012).

If tholeiitic and calc-alkaline arc magmas are equally hydrous, factors other than magmatic $H_2O$ must be invoked to explain the differences between the two series. These include contrasting conditions of magma fractionation (e.g. Green, 1980; Tang et al., 2019) as well as con-trasting parent magma compositions. Adam et al. (2016) argued that the evolution of most arc magmas is governed by low-pressure crystal fractionation involving the magmas' phenocryst phases. But more re-cently Tang et al. (2019) have re-argued the case of Green (1980) for the suppression of Fe enrichment in calc-alkaline magmas by the high-pressure fractionation of garnet ± amphibole. Brounce et al. (2014) have also suggested that differences in oxygen fugacity may cause the separation of the tholeiitic and calc-alkaline series. However, $fO_2$ estimates for the Tongan tholeiites are comparable with those of calc-alkaline magmas examined by Brounce et al. (2014) effectively ne-gating this argument.

A difficulty with any origin involving garnet is that the resulting frac-tionation series should demonstrate a strong positive correlation be-tween Dy/Yb and standard indices of melt fractionation. Yet as demonstrated by the work of Davidson et al. (2007, 2013) this correla-tion is usually negative (see previous discussion of the cryptic amphi-bole model). An alternative possibility involving olivine fractionation from tholeiitic magmas (rather than garnet fractionation from calc-alkaline magmas) derives from the suggestion of Nicholls and Ringwood (1973) that low-pressure melting of hydrous peridotites (within the uppermost mantle) should produce silica-rich tholeiitic melts. Because of the high degrees of melting involved, these melts will be both picritic and Fe-rich, while also depleted in alkalis. Early crystallisation of olivine from these parent melts will rapidly increase Fe/Mg while having little effect on absolute Fe concentrations. Because of their silica-rich nature, more evolved tholeiitic melts (of basaltic an-desite to dacite composition) will have a reaction relationship with oliv-ine and precipitate low-Ca pyroxene(s) and plagioclase instead.

The low alkali concentrations of tholeiitic parent magmas will also influence fractionation trends in two separate ways. The first is demon-strated by plotting two parent magma compositions in the AFM system that have the same Fe/Mg but different total alkalis (Fig. 9). For both parent melts, Fe/Mg in coexisting olivines and pyroxenes will be the same. But within the AFM plane the orientation of the vectors relating liquid and crystal compositions (Fig. 9) will differ depending on differ-ences in the total alkali concentrations of parent melts. Because of this, the crystallisation of olivine and pyroxenes from an alkali-rich parent melt will produce a liquid fractionation trend dominated by strong rel-ative alkali enrichments, but only moderate Fe enrichment (i.e. a calc-alkaline trend). Conversely, the fractionation of an alkali-poor parent melt will be dominated by a strong Fe-enrichment trend as characteris-tic of the tholeiitic series.

The second and separate effect produced by alkalis is akin to the pre-viously cited influence of $H_2O$ on liquidus equilibria. This occurs because the substitution of alkalis for Ca also destabilises plagioclase relative to olivine and pyroxenes (see Adam et al., 2016). Although less commonly referred to, this effect is actually stronger than the more commonly cited influence of $H_2O$. With this context in mind, it is worth recalling the original use of the alkali-lime index by Peacock (1931) to distinguish rocks of “calc-alkalic” type (from which the term “calc-alkaline” ulti-mately derives) from those of alkalic and calcic type.

Finally, we note that a distinct, hydrous primary parent magma for arc tholeiites can help to explain the prominence of tholeiites in the early stages of volcanic arc development. This is because the conditions of parent-magma generation can be linked to the thickness and matu-rity of arc crust. In this case, the early formed tholeiitic parents are the result of comparatively large degrees of melting at shallow depths, whereas the calc-alkaline parent magmas are the result of less extensive but deeper melting. Alternatively or conjunctively, interaction with thickened and evolved crust may produce alkali enrichments and other compositional effects in the later formed calc-alkaline parent magmas (see Farner and Lee, 2017; Green, 1980).

## 5. Conclusions

The results of our experimental study of a basaltic andesite from Late reinforce previous suggestions that Tongan arc magmas differentiate at shallow depths (equivalent to ≤0.2 GPa). Thus crystal fractionation within the upper crust rather than lower crustal melting, is our pre-ferred explanation for the generation of silicic arc magmas in Tonga. Dif-ferentiation is controlled by cotectic relationships involving the erupted volcanics' phenocryst phases (plagioclase + augite ± pigeonite ± orthopyroxene). The dominance of clinopyroxene among the

fractionating ferromagnesians is sufficient to explain the evolutionary trends of REE in the Tongan magma without recourse to cryptic frac-tionation by amphibole (which is notably absent from both our experi-mental run products and the natural Tongan lavas).

The conditions of phenocryst precipitation defined by our experi-ments highlight the hydrous nature of Tongan tholeiitic magmas and contradict some previous proposals regarding the role of $H_2O$ in separat-ing the evolutionary trends of tholeiitic and calc-alkaline magmas. We suggest that these evolutionary trends are principally related to differ-ences in parent magma composition that are unrelated to magmatic $H_2O$.

## Acknowledgements

This research was supported by the Australian Research Council and specifically grant DP110103284 to Tracy Rushmer and Simon Turner.

## References

Adam, J., Turner, S., Rushmer, T., 2016. The genesis of silicic arc magmas in shallow crustal cold zones. Lithos 254, 472–494.

Annen, C., Blundy, J.D., Sparks, R.S.J., 2006. The genesis of intermediate and silicic magmas in deep crustal hot zones. J. Petrol. 47, 505–539.

Arculus, R.J., 2003. Use and abuse of the terms calcalkaline and calkalkalic. J. Petrol. 44, 929–935.

Beier, C., Turner, S.P., Haase, K.M., Pearce, J.A., Münker, C., Regelous, M., 2017. Trace element and Isotope Geochemistry of the Northern and Central Tongan Islands with and Emphasis on the Genesis of high Nb/Ta signatures at the Northern Volcanoes of Tafahi and Niuatoputapu. J. Petrol. 58, 1073–1106.

Bevis, M., Taylor, F.W., Schutz, B.E., Recy, J., Isacks, B.L., Heiu, S., Singh, R., Kendrick, E., Stowell, J., Taylor, B., Calmant, S., 1995. Geodetic observations of very rapid conver-gence and back-arc extension at the Tonga arc. Nature 374, 249–251.

Blatter, D.L., Sisson, T.W., Hankins, W.B., 2013. Crystallisation of oxidised, moderately hydrous arc basalt at mid- to lower-crustal pressures: implications for andesite genesis. Contrib. Mineral. Petrol. 166, 861–886.

Blatter, D.L., Sisson, T.W., Hankins, W.B., 2017. Voluminous arc dacites as amphibole reaction-boundary liquids. Contrib. Mineral. Petrol. 172, 27.

Botcharnikov, R.E., Holtz, F., Behrens, H., 2015. Solubility and fluid-melt partitioning of $H_2O$ and Cl in andesitic magmas as a function of pressure between 50 and 500 MPa. Chem. Geol. 418, 117–131.

Boyd, F.R., England, J.L., 1960. Apparatus for phase-equilibrium measurements at pres-sures up to 50 kilobars and temperatures up to 1750°C. J. Geophys. Res. 65, 741–748.

Brophy, J.G., 2008. A study of rare earth element (REE)-$SiO_2$ variations in felsic liquids generated by basalt fractionation and amphibolite melting: a potential test for dis-criminating between the two different processes. Contrib. Mineral. Petrol. 156, 337–357.

Brounce, M.N., Kelley, K.A., Cottrell, E., 2014. Variations in $Fe^{3+}/\Sigma Fe$ of Mariana Arc Basalts and Mantle Wedge $fO_2$. J. Petrol. 55, 2513–2536.

Bryan, W.B., Stice, G.D., Ewart, A., 1972. Geology, petrography, and geochemistry of the Volcanic Islands of Tonga. J. Geophys. Res. 77, 1566–1585.

Caulfield, J.T., Turner, S.P., Smith, I.E.M., Cooper, L.B., Jenner, G.A., 2012. Magma evolution in the primitive, intra-oceanic Tonga arc: petrogenesis of basaltic andesites at Tofua volcano. J. Petrol. 53, 1197–1230.

Contreras-Reyes, E., Grevemeyer, I., Watts, A.B., Flueh, E.R., Peirce, C., Moeller, S., Papenberg, C., 2011. Deep seismic structure of the Tongan subduction zone: implica-tions for mantle hydration, tectonic erosion, and arc magmatism. J. Geophys. Res. 116, B10103. https://doi.org/10.1029/2011JB008434.

Cooper, L.B., Ruscitto, D.M., Plank, T., Wallace, P.J., Syracuse, E.M., Manning, C.E., 2012. Global variations in $H_2O$/Ce: 1. Slab surface temperatures beneath volcanic arcs. Geochem. Geophys. Geosyst. 13. https://doi.org/10.1029/2011GC003902.

Davidson, J., Turner, S., Handley, H., Macpherson, C., Dosseto, A., 2007. Amphibole "sponge" in arc crust? Geology 35, 787–790.

Davidson, J., Turner, S., Plank, T., 2013. Dy/Dy*: variations arising from mantle sources and Petrogenetic Processes. J. Petrol. 54, 525–537.

Ewart, A., Bryan, W.B., Gill, J.B., 1973. Mineralogy and Geochemistry of the Younger Vol-canic Islands of Tonga, S.W. Pacific. J. Petrol. 14, 429–465.

Farner, M.J., Lee, C.A., 2017. Effects of crustal thickness on magmatic differentiation in subduction zone volcanism: a global study. Earth Planet. Sci. Lett. 470, 96–107.

Fujimaki, H., Tatsumo, M., Aoki, K., 1984. Partition coefficients of Hf, Zr, and REE between phenocrysts and groundmass. J. Geophys. Res. 89, B662–B672.

Gill, J.B., 1981. Orogenic Andesites and Plate Tectonics. Springer, Berlin Heidelberg New York.

Green, D.H., 1976. Experimental testing of "equilibrium" partial melting of peridotite under water-saturated, high-pressure conditions. Can. Mineral. 14, 255–268.

Green, T.H., 1980. Island arc and continent building magmatism – a review of petroge-netic models based on experimental petrology and geochemistry. Tectonophysics 63, 367–385.

Green, T.H., Ringwood, A.E., Major, A., 1966. Friction effects and pressure calibration in a piston-cylinder apparatus at high pressure and temperature. J. Geophys. Res. 71, 3589–3594.

Green, T.H., Sie, S.H., Ryan, C.G., Cousens, D.R., 1989. Proton microprobe-determined partitioning of Nb, Ta, Zr, Sr and Y between garnet, clinopyroxene and basaltic magma at high pressure and temperature. Chem. Geol. 74, 201–216.

Grove, T.L., Elkins-Tanton, L.T., Parman, S.W., Chatterjee, N., Müntener, O., Gaetani, G.A., 2003. Fractional crystallisation and mantle melting controls on calc-alkaline differen-tiation trends. Contrib. Mineral. Petrol. 145, 515–533.

Hamada, M., Fujii, T., 2008. Experimental constrains on the effects of pressure and $H_2O$ on the fractional crystallization of high-Mg island arc basalt. Contrib. Mineral. Petrol. 155, 767–790.

Hamada, M., Okayama, Y., Kaneko, T., Yasuda, A., Fujii, T., 2014. Polybaric crystallization differentiation of $H_2O$-saturated island arc low-K tholeiite magmas: a case study of the Izu-Oshima volcano in the Izu arc. Earth Planets Space 66, 15.

Jakes, P., Gill, J., 1970. Rare Earth elements and the Island Arc Tholeiitic Series. Earth Planet. Sci. Lett. 9, 17–28.

Johnson, R.W., Jaques, A.L., Hickey, R.L., McKee, C.O., Chappell, B.W., 1985. Manam Island, Papua New Guinea: petrology and geochemistry of a low-$TiO_2$ basaltic island-arc vol-cano. J. Petrol. 26, 283–323.

Kuno, H., 1959. Origin of Cenozoic petrographic provinces of Japan and surrounding areas. Bull. Volcanol. 20, 37–76.

Kuno, H., 1968. Differentiation of basalt Magmas. In: Hess, H.H., Poldervaart, A. (Eds.), The Poldervaart Treatise on Rocks of Basaltic Composition. Interscience Publishers, New York, pp. 623–688.

Lindsley, D.H., 1983. Pyroxene thermometry. Am. Mineral. 68, 477–493.

Lindsley, D.H., Andersen, D.J., 1983. A two-pyroxene thermometer. J. Geophys. Res. Solid Earth 88, A887–A906.

Nandedkar, R.H., Ulmer, P., Müntener, O., 2014. Fractional crystallisation of primitive, hy-drous arc magmas: an experimental study at 0.7 GPa. Contrib. Mineral. Petrol. 167, 1015.

Nicholls, I.A., Ringwood, A.E., 1973. Effect of water on olivine stability in tholeiites and the production of silica-saturated magmas in the island-arc environment. J. Geol. 81, 285–300.

O'Hara, M.J., 1968. The bearing of phase equilibria studies in synthetic and natural sys-tems on the origin and evolution of basic and ultrabasic rocks. Earth Sci. Rev. 4, 69–133.

O'Neill, H.S.C., Pownceby, M.I., 1993. Thermodynamic data from redox reactions at high temperatures. I. an experimental and theoretical assessment of the electrochemical method using stabilised zirconia electrolytes, with revised values for the Fe-"FeO", Co-CoO, NiNiO and Cu-Cu2O oxygen buffers, and new data for the W-WO2 buffer. Contrib. Mineral. Petrol. 114, 296–314.

O'Neill, H.S.C., Berry, A.J., Mallmann, G., 2018. The oxidation state of iron in Mid-Ocean Ridge Basaltic (MORB) glasses: implications for their petrogenesis and oxygen fugac-ity. Earth Planet. Sci. Lett. 504, 152–162.

Parman, S.W., Grove, T.L., Kelley, K.A., Plank, T., 2011. Along-arc variations in the pre-eruptive $H_2O$ contents of Mariana Arc magmas inferred from fractionation paths. J. Petrol. 52, 257–278.

Peacock, M.A., 1931. Classification of igneous rocks series. J. Geol. 39, 54–67.

Putirka, K., 2008. Thermometers and barometers for volcanic systems. Rev. Mineral. Geochem. 69, 61–120.

Smith, D.J., 2014. Clinopyroxene precursors to amphibole sponge in arc crust. Nat. Commun. 5, 4329.

Smith, I.E.M., Price, R.C., 2006. The Tonga-Kermadec arc and Havre-Lau back-arc system: their role in the development of tectonic and magmatic models for the western Pa-cific. J. Volcanol. Geotherm. Res. 156, 315–331.

Tang, M., Lee, C.-T.,.A., Erdman, M., Costin, G., Jiang, H., 2019. Nb/Ta systematics in arc magma differentiation and the role of arcogites in continent formation. Nat. Commun. 10, 235.

Tatsumi, Y., Suzuki, T., 2009. Tholeiitic vs Calc-alkaline differentiation and evolution of Arc Crust: constrains from melting experiments on a Basalt from the Izu-Bonin-Mariana Arc. J. Petrol. 50, 1575–1603.

Turner, S.P., George, R., Jerram, D.A., Carpenter, N., Hawkesworth, C., 2003. Case studies of plagioclase growth and residence times in island arc lavas from Tonga and the Lesser Antilles, and a model to reconcile discordant age information. Earth Planet. Sci. Lett. 214, 279–294.

Turner, S., Caulfield, J., Rushmer, T., Turner, M., Cronin, S., Smith, I., Handley, H., 2012. Magma evolution in the primitive, Intra-oceanic Tonga arc: Rapid Petrogenesis of Dacites at Fonualei Volcano. J. Petrol. 53, 1231–1253.

Wilkinson, J.F.G., 1967. The petrography of the basaltic rocks. In: Hess, H.H., Poldervaart, A. (Eds.), The Poldervaart Treatise on Rocks of Basaltic Composition. Interscience Pub-lishers, New York, pp. 163–214.

Wood, B.J., Blundy, J.D., 1997. A predictive model for rare earth element partitioning be-tween clinopyroxene and anhydrous silicate melt. Contrib. Mineral. Petrol. 129, 166–181.

Zimmer, M.M., Plank, T., Hauri, E.H., Yogodzinski, G.M., Stelling, P., Larsen, J., Singer, B., Jicha, B., Mandeville, C., Nye, C.J., 2010. The role of water in generating the Calc-alkaline trend: new volatile data for aleutian magmas and a new tholeiitic index. J. Petrol. 51, 2411–2444.